Muon Lifetime and Muon Mass

Alex Leonardi[1, 2, *] and Inko Bovenzi[1, 3, †]

[1] *Department of Physics, Harvard University, Cambridge, Massachusetts 02138, USA*
[2] *Department of Mathematics, Harvard University, Cambridge, Massachusetts 02138, USA*
[3] *Department of Computer Science, Harvard University, Cambridge, Massachusetts 02138, USA*

(Dated: May 24, 2025)

We measure the lifetime and mass of cosmic ray muons. We use three plastic scintillators to catch muons and a mix of logic gates and discriminators to isolate muons that are caught by the middle scintillator and later decay. Over the course of 110,000 decay observations, we achieve a reasonable lifetime estimate of 2.17(2) μs, comparable to the accepted value of 2.2 μs, though there is potential for substantial systematic error. We then measure the mass of the muon by analyzing the distribution of energies of electrons produced by the decay of the muons. We estimate the mass of the muon to be 106.4(6.4) MeV, consistent with the accepted value of 105.66 MeV. These results demonstrate that a system of three scintillators can be used to accurately assess the lifetime and mass of muons, which has several applications, most notably in estimating the weak force coupling constant and muon radiography.

I. INTRODUCTION

Carl D. Anderson and Seth H. Neddermeyer discovered the muon in 1936 [1] [2]. J.C. Street and E.C. Stevenson independently confirmed this discovery shortly after [3]. The muon (μ^-) is a negatively charged elementary particle with a mass of 105.6583755(23) MeV [4]. The mass of an electron is almost 207 times smaller than the mass of the muon [4].

Cosmic radiation is the main source of muons we detect on Earth. Victor Hess discovered cosmic rays in 1912 and his work won the Nobel Prize in 1936 [5]. Cosmic rays originate from astrophysical processes like the sun or supernovae and consist of 90% hydrogen, 9% helium, and 1% all other natural elements [6]. The incoming protons (hydrogen) in the cosmic ray interact with Earth's atmosphere to produce charged mesons (pions) that then decay into muons and neutrinos [7].

Pions ($\pi^{\pm}$) exhibit the following decay process,

$$\pi^- \to \mu^- + \bar{\nu}_\mu$$
$$\pi^+ \to \mu^+ + \nu_\mu$$

where μ^+ are anti-muons, ν_μ are muon neutrinos, and $\bar{\nu}$ are anti-neutrinos [8]. Many muons reach the surface of the Earth despite passing through Earth's atmosphere [7]. The survival probability of a subatomic particle is modeled as a Poisson process and gives the probability of the particle lasting for time t_0 or greater as,

$$P(t_0) = e^{-t_0/(\tau\gamma)} = e^{-Mt_0/(\tau E)} \tag{1}$$

where we consider the momentum of the particle given by the four-vector $(E, \vec{p})$, proper lifetime τ, Lorentz factor γ, and mass of the particle M [9]. The accepted value for the mean lifetime of the muon is 2.1969811(22) μs [4]. The probability the particle travels a distance x_0 is

$$P(x_0) = e^{-Mx_0/(|\vec{p}|\tau)}, \tag{2}$$

and so from Eqns. (1) and (2) we expect to observe negative exponential distributions in the data from our experiment. The Lorentz factor from special relativity,

$$\gamma = \frac{1}{\sqrt{1 - \frac{v^2}{c^2}}},$$

grows as the velocity v increases. We note that the rest frame does not consider this γ factor,

$$\begin{aligned} x_{\text{muon rest frame}} &= v\tau \\ &\approx (299,792,458 \text{ m/s})(2.1969811\ \mu\text{s}) \\ &\approx 658.63836 \text{ m}, \end{aligned}$$

which is why we may be suprised that muons travel far enough to reach the surface of the Earth. Yet taking into account that muons travel at nearly the speed of light c [10], this γ is then close to its maximal value, meaning that in the Earth frame the muons can travel a great distance:

$$\begin{aligned} x_{\text{Earth frame}} &= v\tau\gamma \\ &= (299,792,458 \text{ m/s})(2.1969811\ \mu\text{s})\ \gamma \\ &\geq 2.6345534 \text{ km when } \gamma \geq 4. \end{aligned}$$

Thus, after examining that $x_{\text{Earth}} = v\tau\gamma = \frac{|\vec{p}|\tau}{M}$, we realize without the γ factor, the exponential decay in Eqn. (2) would occur so quickly that few muons would reach Earth's surface [11] [12]. Since muons only interact through the weak force [13], they have a longer lifetime than pions, which allows them to last long enough for us to detect with this experiment.

Muons decay into three particles. The first particle is an electron or positron, while the other two are a neutrino

* alexleonardi@college.harvard.edu
† ibovenzi@college.harvard.edu

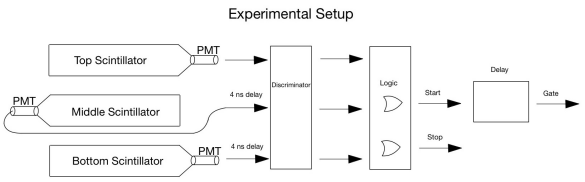

FIG. 1. Progression of electrical signals within the experimental setup.

and anti-neutrino pair:

$$\mu^- \to e^- + \nu_\mu + \bar{\nu}_e$$
$$\mu^+ \to e^+ + \nu_e + \bar{\nu}_\mu$$

where $e^\mp$ are electrons and positrons, and ν_e are electron neutrinos [13]. By energy conservation, the mass of the muon is equal to the sum of the energies of the three particles that a muon at rest decays into:

$$m_\mu c^2 = E_{e^\pm} + E_{\nu_{e,\mu}} + E_{\overline{\nu}_{\mu,e}} \tag{3}$$

The energy of these particles is mainly kinetic because the mass of the electron, the neutrino, and the anti-neutrino are very small compared to the mass of the muon. We also have conservation of momentum:

$$\vec{p}_{e^\pm} + \vec{p}_{\nu_{e,\mu}} + \vec{p}_{\overline{\nu}_{\mu,e}} = 0 \tag{4}$$

Accurate measurements of this lifetime and the muon mass allow us to better determine the weak force coupling constant [14] as in Equation 5. These measurements can also help with important uses of muons, such as detecting damage in nuclear reactors [15].

$$\frac{1}{\tau_\mu} = \frac{G_F^2 m_\mu^5}{192\pi^3} \tag{5}$$

II. SETUP

A. General Setup

Many experiments have been proposed to measure the lifetime of muons using a setup similar to ours [16] [17] [18]. A plastic scintillator, photomultiplier tube (PMT), and discriminator setup can detect muons and measure the lifetime of muons that stop in the apparatus. Figure 1 shows our setup, and Appendix A shows a more detailed diagram of all of the components. (The muon lifetime can also be measured using a multiplate spark chamber setup, as described in [19].)

Owens and MacGregor demonstrated that a single scintillator connected to a PMT and discriminator perform more than 100 detections an hour and that this is sufficient to calculate the muon lifetime [17]. Our experiment setup was similar, though we employed three scintillators rather than one, to aid in discriminating noise in the pulses and PMT aftershocks (secondary signals in any given PMT following a muon detection, typically within 1 μs). The PMT amplifies and sends the photon signal to the discriminator, where a series of logic gates are used to enforce a threshold that determines whether the pulse contained enough energy to be classified as a muon. When a muon is trapped in a scintillator, the PMT also amplifies a second pulse from the muon decaying into an electron. We used the second pulse as our stopping condition to measure decays. An oscilloscope displays the time between pulses and a computer collects this data to calculate and plot the lifetime of the muons that the apparatus detects. By measuring the energy of the particle resulting in the second pulse, we can also calculate the mass of the muon. Given the accepted cosmic muon flux of 1 muon per cm^2 per minute, we estimate that 80 muons would flow through our detectors every second.

In this setup, we delayed the outputs from the top and bottom scintillators by 4 ns so that the three signals would arrive as concurrently as possible. This delay may have been necessary due to a longer wire used for the middle scintillator, which slowed the signal. Without this delay, parts of the logic would fail on the front/tail end of the signals. We chose our high voltage and discriminator thresholds for each PMT in an iterative testing process to optimize muon detection rates while minimizing noise. A full description of this process can be found in Appendix B.

B. Logic Gates

We use the logic gates to generate a start and stop signal. Throughout this paper, in our logic notation, T stands for the top scintillator, M the middle, and B the bottom. The start signal is $T \wedge M \wedge \bar{B}$, indicating that a muon has been captured in the middle detector. Once the muon decays, it will release an electron either upwards or downwards, meaning that our stopping signals are $T \wedge M \wedge \bar{B}$ or $\bar{T} \wedge M \wedge B$. The logic is shown in Figure 2. This setup does leave open the possibility that an electron will be released horizontally without clipping the bottom or top detectors. In these cases, we will miss the decay. We triggered a muon detection when the $20\mu s$ gate initiated by a start signal coincides with a stop signal. As shown in Figure 3, we delayed that gate by $100ns$ to prevent double signals from a long start pulse because start signals can be misinterpreted as stop signals.

Once the oscilloscope detected a stop signal, we recorded the previous 20 μs of data and recorded a muon. The difference in start and stop times became the measured lifetime. We ran this experiment over the course of three weeks and captured 110, 000 muons. We expected that around $1.5 \cdot 10^8$ muons would reach at least the top

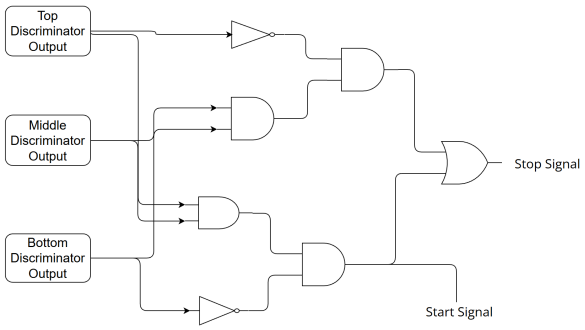

FIG. 2. Experiment logic gates. This shows the setup for the starting and stopping conditions.

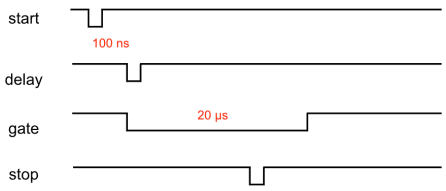

FIG. 3. Delay and gate setup. We trigger muon detection on a stop AND gate signal. We used a delay since the starting signal is also a stopping signal.

detector over the course of those three weeks, so around .1% of the muons became stuck in the middle scintillator.

III. MUON LIFETIME MEASUREMENT

Our muon lifetime data most closely resembles the sum of a negative exponential distribution and a constant. The exponential distribution component of this makes sense; that is how muons decay. The constant can be explained by a "dark count" present in the data that is approximately evenly distributed across all lifetime values. There are a number of factors that may explain the dark count, which accounts for around 15% of the data. First, the delay gate means the muons with a lifetime of under 100 ns are never seen, and after they trigger a start signal, random pulses in the scintillators could create a phantom count. We expect to miss around 4.5% of the muons through these early decays. Second, in general, pulses through the circuits could lead to errant stop or start signals. Third, the signal from the decay of a muon could be missed if the discriminator threshold is too high, leading to a secondary signal being picked up. Fourth, muons whose electrons decay horizontally will not have a stop signal, and as in the first reason, there could be an errant later stopping signal. All four of these error sources would lead to an equal likelihood of detection for any lifetime under 20 μs, so the dark count is likely constant.

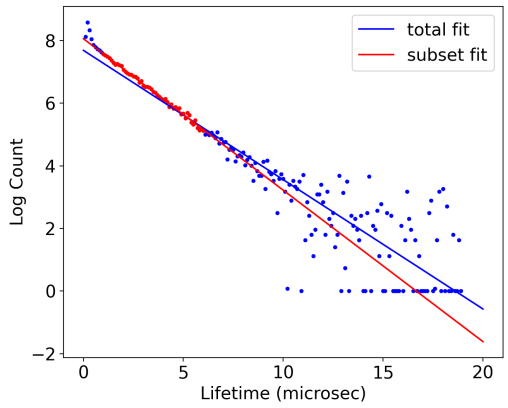

FIG. 4. Linear fit of log(count). The subset fit is on the range [1,6] μs. The cluster of points around 0 represent points with counts below the dark count threshold. The subset line fits the subset data much better than the total fit.

A. Curve Fit

Figure 4 shows the results of subtracting out the dark count and then taking the log of count data. The figure shows how the dark count injects a lot of noise into the results past a lifetime of 6 μs. We can also see that the first few data points seem to be above the linear trend line, likely the result of PMT aftershocks occurring within 1 μs of the muon arrival. Therefore, the subset line, which only considers data points within the lifetime range $[1, 6]$, fits the early, high-sample size data much better.

In Figure 5, we display the results of our exponential + constant fit for the whole data and data subset. We fit the following equation, where y is the count, t is the lifetime, a is a scaling factor, c represents the dark count, and b represents the lifetime. Our fit gave $a = 7190$, $b = 2.17$ μs, and $c = 292$.

$$y = c + a \cdot e^{-t/b} \tag{6}$$

We prefer this fit for our final analysis because it avoids the cluster of 0s in Figure 4 that occurs from subtracting the dark count. The data subset yields a measured lifetime of 2.17 μs.

When regressing on Equation 6 we estimated the statistical error in the measurement of each data point to capture the different errors in each measurement appropriately.

Given the sum of the two distributions, we can estimate the error in each and then take the Pythagorean distance of the two errors. Where m is the number of true measurements, λ is the dark count, and $m + \lambda = n$ is the sample size, the standard deviation of the true count in a certain bin goes as $m/\sqrt{m} = \sqrt{m}$. We estimate the error of the constant distribution as that of a Poisson distribution by estimating the frequency of these observations at the end of the tail with few muons and then using the

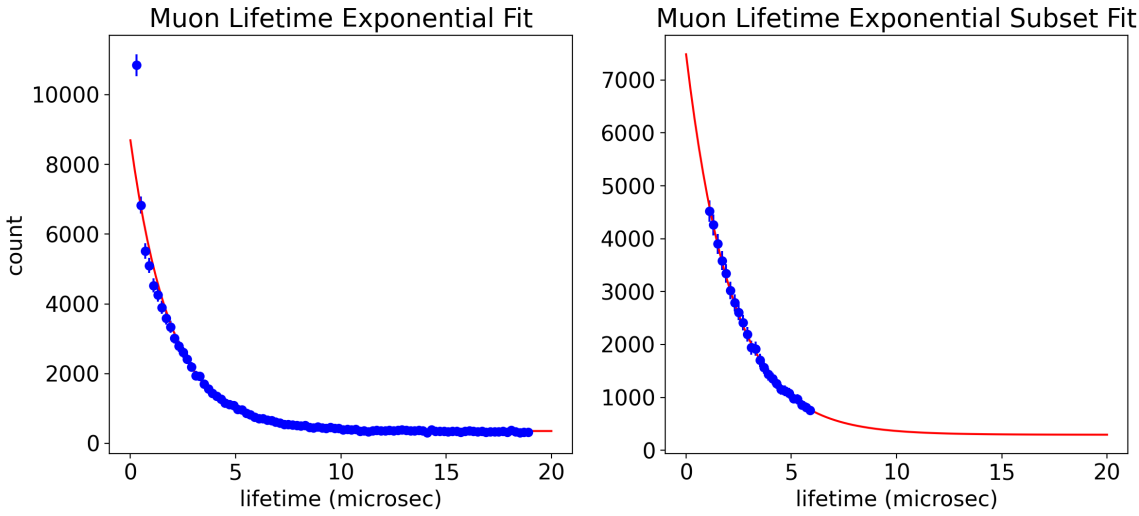

FIG. 5. Exponential + constant fits for muon lifetimes. The first panel has the full data; the second panel is a subset of the range [1,6] μs. The fit quality is higher in the second panel. Error bars represent 3σ of statistical error. Our measured lifetime is 2.17μs.

Poisson distribution standard deviation: $\sqrt{\lambda}$, where λ is the rate parameter. Overall, we calculated the statistical error on each point as: $\sqrt{m+\lambda} = \sqrt{n}$. In this way, we do not need to know the value of m or λ for the fit.

We check the sensitivity of our results to the hyper-parameters of bin size, starting threshold, and ending threshold (which in our fit were .1, 1, and 6 respectively) in Figure 6 and Figure 7. In an ideal scenario, reasonable variations in the bin size should not matter because the data remains the same with any bin size, though we checked this for completeness.

As can be seen in **??**, the first data point is well above the distribution, and is several standard deviations away from the fit. We thought that PMT aftershocks were possibly causing errant measurements under 1 μs, but they should generally end after that time window. For high lifetimes, the signal-to-noise ratio seems to fall around 6 or 7μs, suggesting that including the rest of the dark-count-dominated data would only increase noise. It is worth noting that past experiments have also had very noisy back ends of their distributions, though typically at higher time values than our experiment (~12 μs) [18].

Consider that the mean number of observations at any point in time corresponds exactly to the number of items in each bin. We have that bins contain $\bar{x}$ items and $\bar{x}$ is proportional to the total number of events n. From this, we see that the standard deviation on the signal is proportional to the square root of the overall count, $\sigma_{\text{signal}} \sim \sqrt{n}$. Since we model the dark count using a Poisson distribution, the dark count is λ per bin and the standard deviation of the noise is $\sigma_{\text{noise}} \sim \sqrt{\lambda}$. Since $\lambda \sim n$, then $\sigma_{\text{noise}} \sim \sqrt{n}$. Thus, the signal to noise ratio is constant for any value of n. Since we expect the SNR to remain constant, we expect that the heat map does not shift in Figure 7 if we were to collect more data.

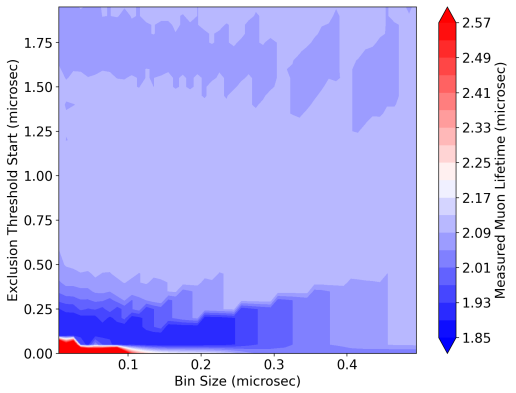

FIG. 6. A contour plot of our measured lifetimes over a series of bin sizes and starting thresholds. Bin size does not seem to have a major impact.

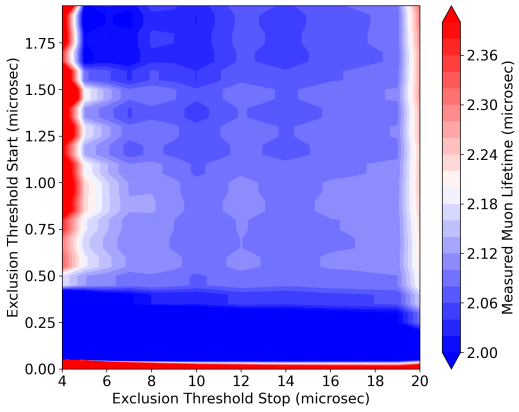

FIG. 7. A contour plot of our measured lifetimes over a series of ending and starting thresholds.

B. Confidence Intervals / Significance

There are two sources of error to account for: statistical error in the fit and systematic error inherent to the experiment. We accounted for statistical error in the standard calculation for a counting experiment measuring a negative exponential distribution, calculating the 95% confidence interval as $2.17 \pm 2.17 \cdot \frac{1.96}{\sqrt{n}} \mu$s. Though our sample size is roughly 110,000 muons, the [1,6] subset of our fit has 75,000 muons, so our range is $2.17 \pm .016$ μs. To verify this result, we performed bootstrapping (taking random subsets of our [1,6] data and comparing the results to each other to estimate statistical error). Keeping 40% of the data and rejecting the rest at random produced a standard deviation in the measured lifetime of .014 μs; keeping 80% of the data resulted in a standard deviation of .006 μs (both performed over 10,000 iterations). These results are largely consistent with our calculated value for the 95% confidence interval.

The larger source of error is the systematic error from the setup and the selection of our fit hyper-parameters. One way to estimate this error is to assess how much the measured lifetime varies with reasonable selections of bin size, starting threshold, and stopping threshold. We estimate the maximum error from bin size selection to be .04 μs based on Figure 6. The choice of the starting threshold across reasonable values in Figure 7 that avoid most PMT aftershocks can result in variation of up to .1 μs as the gradient at certain points is quite sharp, whereas the stopping value can change the result from 2.12 to 2.3 μs. Altogether, there is room for substantial systematic error in the experiment, as the three hyper-parameters can introduce 2%, 5%, and 9% errors. We think that this encompasses nearly the full extent of systematic error in the experiment though because the hyper-parameters can tune out the other most likely sources of error: the dark count and PMT aftershocks. Combining the statistical error with these estimates, we calculate the total error to be 13.8%, so our measurement is 2.17(29) μs. However, we selected the hyper-parameters with a clear rationale to limit the influence of other errors, so this error is a high estimate.

IV. MUON MASS MEASUREMENT

A. Data Collection and Calculation

Our setup for the muon mass experiment was similar to that of the lifetime experiment, except that we also recorded the strength of the decay signals from electrons in the middle scintillator (by looking at the amplitude of the PMT output). These strengths were measured in volts, but we used them to calculate the momentum of the electrons.

To calculate the mass of the muons, we still need one more piece of data because we have the electron data in volts instead of energy. Therefore, we need to run a mass calibration trial. The mass calibration experiment examines muons that pass through all three detectors and measures the size of the raw voltage induced in the middle scintillator. Thus, we measure the voltage created by a minimum-ionizing muon using the high-energy cutoff of Figure 8. See Appendix C for more details.

Lastly, we need a method of converting the measured voltages to energies. Figure 9 shows the muon mass stopping power for a series of elements as modeled by the Bethe equation in Appendix D. Thus, we use the results of Figure 9 to convert the voltages of minimum-ionizing muons to energies. Using that energy data, by conservation of energy in Equation 3, we can say that half of the kinetic energy in a maximum-energy-electron scenario is stored in the electron, and thus, twice that energy represents the mass of the muon.

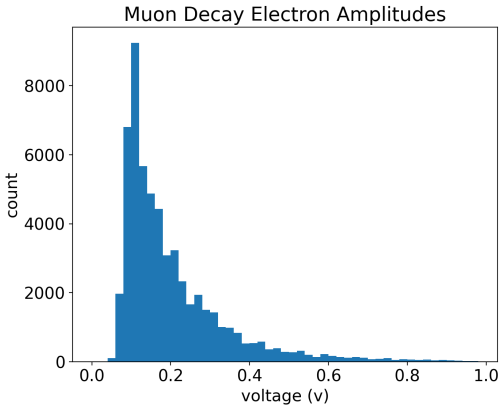

FIG. 8. Muon mass measurements. We measure the amplitude of PMT signals for muon decays to understand the high-energy cutoff for electrons produced by these decays.

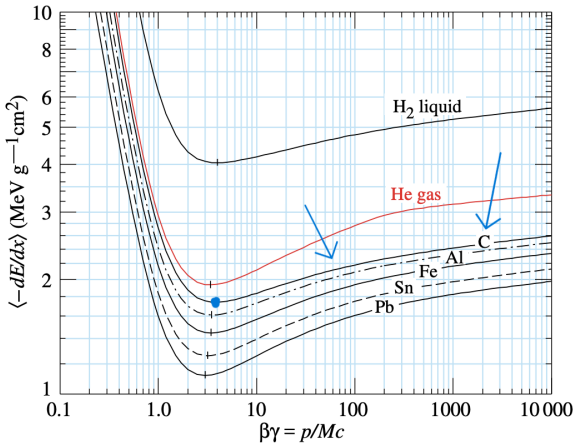

FIG. 9. Muon mass stopping power $\left\langle -\frac{dE}{dx} \right\rangle$ from the Particle Data Group. Different lines show the result for different materials, including for carbon (blue arrows; minimum-ionizing energy marked with a dot). Carbon is relevant to our experiment since the scintillator is plastic. [20]

Using this information, we can calculate the muon mass as follows:

$$m = \frac{2v_m}{v_p}\left(\left\langle -\frac{\partial E}{\partial x}\right\rangle\Bigg|_{\text{min ion}}\right)\rho w \tag{7}$$

m is the mass of the muon, v_m is the maximum electron voltage, v_p is the calibration voltage of a minimum-ionizing muon, ρ is the density of the scintillator, w is the thickness of the scintillator, and $\left\langle -\frac{\partial E}{\partial x}\right\rangle$ is taken for a minimum-ionizing muon and is calculated per unit density of the material.

We perform the numerical calculation of Eqn. (6) in Appendix D to find a muon mass of 106.43 MeV, while the accepted value of the muon mass is 105.66 MeV [21].

B. Confidence Intervals / Significance

Given that the mass calculation has many terms, we calculate the estimated maximum error of each measurement and then estimate the final error. The error associated with mass calibration is 5%, given the imprecision in selecting the maximum of the distribution. Our value for the density of the scintillator assumed that the plastic was composed in equal parts of its two listed components (so we averaged their densities), but a different weighting could produce a difference of 2%. We deemed all other measurements, including reading from graphs, to be at worst 1% measurements. Given these specifications, our final estimate of the muon mass is 106.4(6.4) MeV. It is worth noting that there may have been larger, systematic error in assessing the high-energy cutoff in the muon decay distribution from Figure 8. However, as can be seen in the log plots of Figure 13, that cutoff was fairly clean, so the error from here could not have been larger than 5%.

V. CONCLUSIONS AND IMPLICATIONS

We demonstrate that plastic scintillators can be used to measure the muon lifetime and mass with reasonably high accuracy. Future experiments of a similar setup may attempt to choose more stringent thresholds for high voltages and discriminators to lessen the dark count and PMT aftershocks, which were the main sources of error (see Appendix B for more details). These changes would require a longer time frame for the experiment, but it may be worth the greater accuracy.

Knowing the lifetime and mass of muons to a high degree of accuracy is critical to muon radiography imaging techniques in the modern world. Researchers can probe the physical properties of an object by placing muon detectors on either side and measuring the scattering of muons as they pass through the object. This method gives a high-quality image of the scanned object, with especially reliable measurements for materials with high atomic numbers (because their muon-stopping power is higher). Thus, scientists proposed using muon imaging to locate loose uranium after the 2011 Fukushima disaster in Japan [15]. Since the method is non-invasive and naturally occurring muons do not deteriorate delicate materials, similar methods have been used to image the Pyramids of Giza. Such work would not be possible without a strong understanding of muons' physical quantities.

APPENDIX

A. Experimental Setup and Equipment

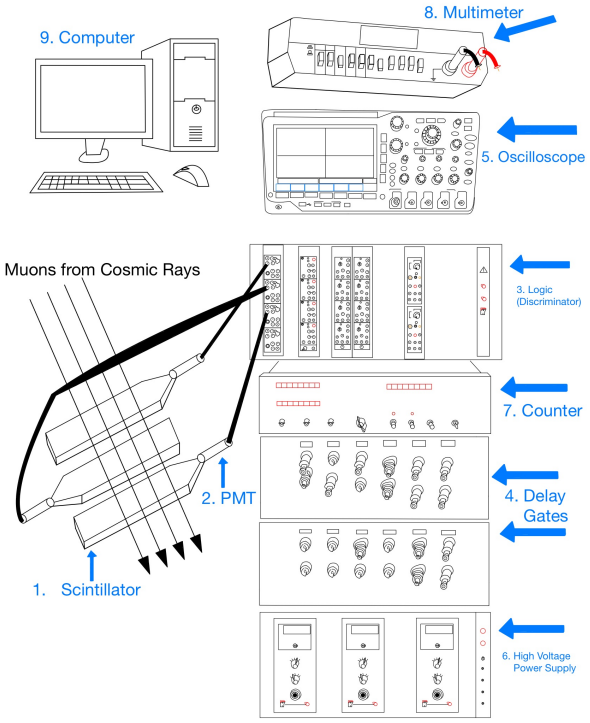

FIG. 10. Experiment equipment. 1. Scintillators are exposed to muons from cosmic radiation. 2. The PMT amplifies the signal and a cable connects each PMT to a Fan-out gate in the Logic section. 3. Logic using AND and OR gates create the boolean expressions to detect if signals were muons. 4. Delay gates are used to ensure we detect signals from each PMT arrive at the same time. 5. An oscilloscope displays the signals. 6. The high voltage power supply allows us to change the voltage and establish thresholds. 7. The counter takes boolean logic and counts the output, providing us with the number of detected muons. 8. The multimeter allows us to measure the change in the voltage of the threshold values we set in the discriminator. 9. The computer receives input from the oscilloscope and plots the data in LabView.

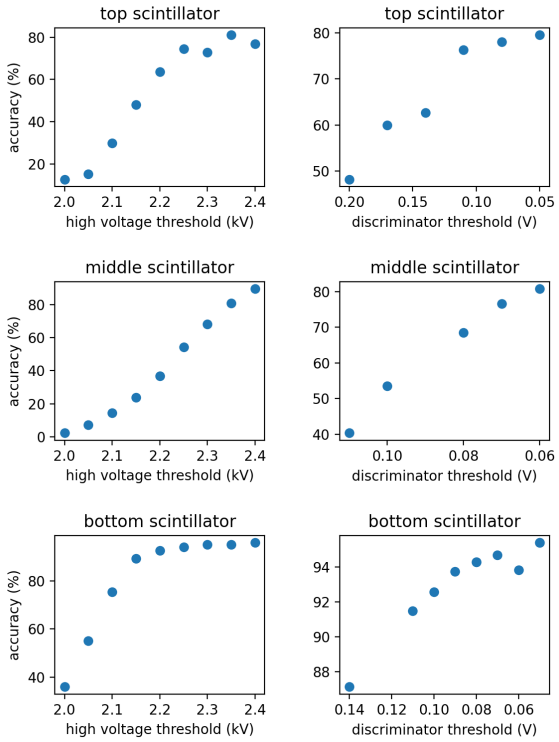

FIG. 11. Selection of high voltage and discriminator thresholds for each of the scintillators. We selected the cutoffs at the point the curves flatten, as further increases in high voltage or decreases in the discriminator values would worsen the signal-to-noise ratio.

B. High Voltage and Discriminator Thresholds

Before running the experiment, it was important to calibrate the high voltage thresholds used for the PMTs and the discriminator thresholds to reject signals with too low of a pulse. We tested a range of plausible high-voltage values and discriminator thresholds to see which values yielded the highest efficiency. We measured efficiency as the ratio of muons seen by all three detectors to the ones seen by the two detectors not being optimized. For example, to optimize the bottom detector, the efficiency would be measured as the ratio $\frac{B \wedge M \wedge T}{M \wedge T}$. Higher high voltage values and lower discriminator values would lead to strictly higher efficiencies, given they allow more detections. Our results are in Figure 11. We chose our thresholds based on where we saw diminishing returns in the improvement of the efficiency. In general, we looked for a plateau in the efficiency/variable graphs, but when one was not present, we chose the inflection point. We took efficiency data for 60 s in each case, which amounted to around 3,000 observations.

We began by setting all the discriminator thresholds to a value of 110 mV. The allowed range for the power sources was 2.00 kV to 2.40 kV, so we tested in increments of 0.05 kV to see if there was a plateau in the efficiency. For the bottom scintillator, we found a clear plateau occurring for a discriminator threshold of 110 mV and a power output of 2.25 kV, with the discriminator threshold held constant for the middle and top scintillators, and power outputs placed at 2.20 kV for both. We then found the bottom discriminator threshold by sweeping through values between 50 and 200 mV, selecting 110 mV.

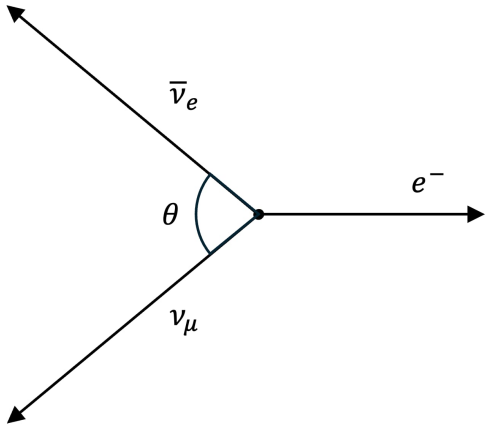

FIG. 12. Muon decay example in two dimensions, as viewed in the rest frame of the muon. The magnitude of the momentum of the electron is fixed by the value of θ.

While working on the middle scintillator, we had trouble finding clean plateaus for high voltage values and discriminator values. We ended up needing to lower the discriminator to 70 mV to find a plateau at 2.35 kV. We used the discriminator threshold of 70 mV given the sensitivity of this result. The top scintillator had fairly clear plateaus at 2.2 kV for the high voltage value and 80 mV for the discriminator.

If we had to do this section again with more time, we would have considered implementing a full grid search to find the highest accuracy pair of high voltage and discriminator values for each detector. Our initial assumption was that the impact of high voltage and discriminator values on accuracy would be independent. However, the results of the middle scintillator suggest that there is co-dependency, meaning that the best plateaus can only be found with a grid search. Such a grid search would have taken around 5 hours to complete with a reasonably fine-grained search, which is why we did not attempt it (3 scintillators, 10 high voltage values, 10 discriminator values, 1 minute for each trial).

C. Mass Calibration

Before taking and analyzing mass calibration data, we modeled the electron voltage distribution. The setup measures the momentum of the electron, and therefore, the distribution of outcomes should resemble the distri-

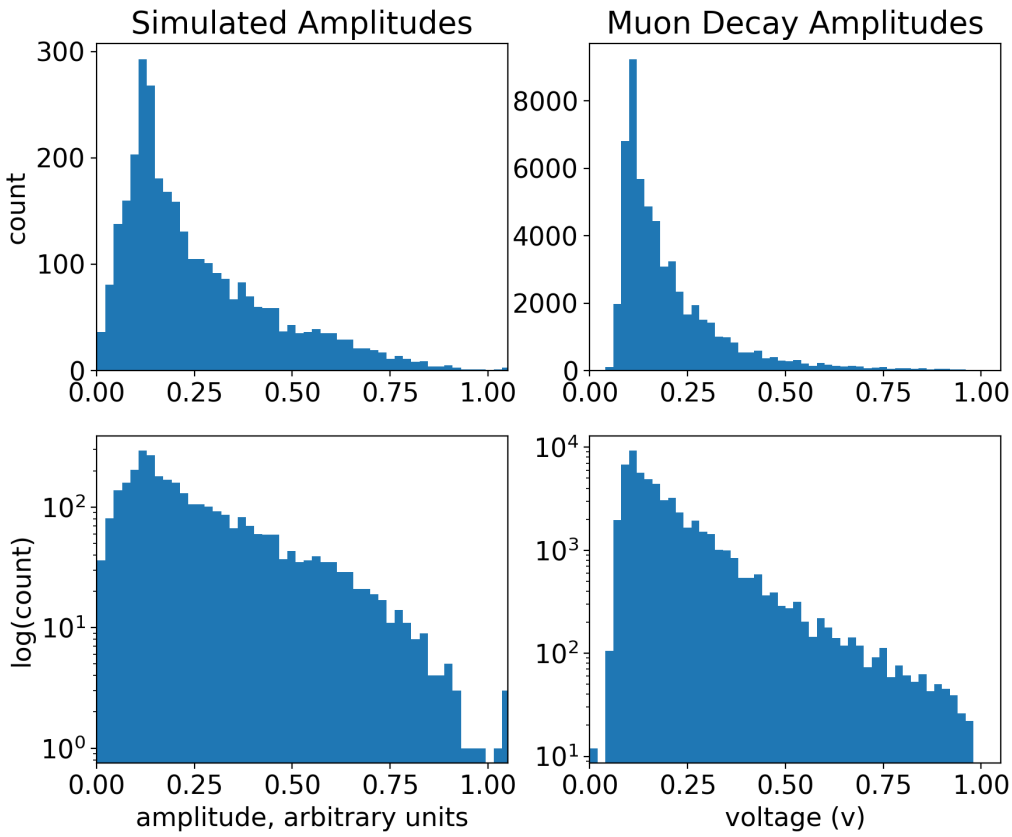

FIG. 13. Using the geometry of the muon decays, we simulated a distribution of how the electron energies may look. The results are close to the muon mass calibration data. We look for the peak value of this distribution to calculate the voltage of a minimum-ionizing muon. The experimental data likely looks cut off at 0 because near-0-energy electrons cannot be measured.

bution of electron momenta post decay. Figure 12 shows an example of how muons may decay into three particles.

Assuming the two neutrinos fly in randomly selected directions, the momentum of the electron is fixed by the relative angle of the neutrinos, and, most importantly, its distribution of momenta can be simulated. The momenta of the three particles must sum to 0 because the captured muons are at rest, and we have conservation of momentum as in Equation 4. By randomly generating angles for the two neutrinos and calculating the resulting electron momentum, we used the geometry of the problem to simulate possible electron data. Electron detectors can detect the share of momentum in a certain fixed direction, so we incorporate this dependency on the angle of incoming electrons to produce the results in Figure 13 (for example, if a given detector points in the x-direction, only p_x is measured).

This toy model of electron decay is useful because our goal is to extract the high-energy cutoff of the electron pulse data in Figure 8. The right side of the distribution is hard to decipher (and may be dominated by errant measurements), so knowing what the distribution should look like helped to arrive at a high-energy cutoff. We also filtered lifetime values over 6 μs to avoid potential dark count muons, but the results did not change.

D. Mass Calculation

We explicitly calculate the muon mass using Eqn. (6),

$$m = \frac{2v_m}{v_p}\left(\left\langle -\frac{\partial E}{\partial x}\right\rangle\Big|_{\text{min ion}}\right)\rho w, \tag{6}$$

by performing the following substitutions. We divide $v_m = 0.98$ V by $v_p = 0.10$ V because this gives the maximum voltage of the electron from the mass data experiment divided by the peak of the mass calibration distribution. We then multiply by $\left\langle -\frac{dE}{dx}\right\rangle = 1.78$ MeV cm^2/g, where this value is read from Figure 9. To fix the units, we need to multiply by the density of the plastic scintillator and its thickness, which makes sense because a wider and denser scintillator would increase the total mass stopping power. The scintillator is composed of both polystyrene and p-terphenyl, and since we were not informed of the exact percent compositions, we averaged the densities of polystyrene, 1.04 g/cm^3, and p-terphenyl

1.24 g/cm^3 to set $\rho = 1.14$ g/cm^3. We measured the width of the middle scintillator as $w = 2.68$ cm using digital calipers. Substituting these values into the equation yields a muon mass of 106.43 MeV.

E. Bethe-Bloch Equation

The Bethe-Bloch Equation gives the mean stopping power as,

$$\left\langle -\frac{dE}{dx} \right\rangle = Kz^2 \frac{Z}{A} \frac{1}{\beta^2} \left(\frac{1}{2} \ln \left(\frac{2m_e c^2 \beta^2 \gamma^2 W_{max}}{I^2} \right) - \beta^2 - \frac{\delta(\beta\gamma)}{2} \right)$$

which is due to the mean energy loss of a particle as it passes through a material. Here $W_{\max}$ is the maximum kinetic energy a free electron can gain from a single collision, E is the incident particle energy, I is the mean excitation energy, Z is the atomic number of absorber, A is the atomic mass of the absorber, and δ is the density effect correction to the ionization loss. A plot of the equation is given in Figure 9. A detailed description of the effects of the Bethe-Bloch equation, including correction terms that modify it, can be found in [20].

[1] C. D. Anderson and S. H. Neddermeyer, Cloud chamber observations of cosmic rays at 4300 meters elevation and near sea-level, Phys. Rev. **50**, 263 (1936).

[2] S. H. Neddermeyer and C. D. Anderson, Note on the Nature of Cosmic Ray Particles, Phys. Rev. **51**, 884 (1937).

[3] J. C. Street and E. C. Stevenson, New evidence for the existence of a particle of mass intermediate between the proton and electron, Phys. Rev. **52**, 1003 (1937).

[4] S. e. a. Navas (Particle Data Group Collaboration), Review of particle physics, Phys. Rev. D **110**, 030001 (2024), p.28.

[5] Nobel Prize Outreach, Award ceremony speech (1936), awarded to Victor Hess in Dec 1936. Accessed: 03-05-2025.

[6] Goddard Space Flight Center (NASA), Cosmic Rays (2017), last updated in July 2017. Accessed: 2025-03-05.

[7] T. Gaisser, T. Stanev, P. Sokolsky, and R. Streitmatter, Cosmic Rays, (2005), revised March 2002 by T.K. Gaisser and T. Stanev (Bartol Research Inst., Univ. of Delaware); revised September 2005 by P.V. Sokolsky (Univ. of Utah) and R.E. Streitmatter (NASA).

[8] D. J. Griffiths, *Introduction to Elementary Particles*, 2nd ed. (Wiley-VCH, Weinheim, Germany, 2012) p. 321, pion Decay.

[9] J. Jackson, Kinematics, in *Review of Particle Physics* (Particle Data Group, Lawrence Berkeley National Laboratory, 2005) p. 2, revised January 2000.

[10] U.S. Department of Energy, Office of Science, Doe explains...muons, accessed: 2025-04-19.

[11] L. Liu and P. Solis, The speed and lifetime of cosmic ray muons, Physics Department, Massachusetts Institute of Technology, Cambridge, MA **2139** (2007).

[12] B. Rossi, K. Greisen, J. C. Stearns, D. K. Froman, and P. G. Koontz, Further measurements of the mesotron lifetime, Phys. Rev. **61**, 675 (1942).

[13] D. J. Griffiths, *Introduction to Elementary Particles*, 2nd ed. (Wiley-VCH, Weinheim, Germany, 2012) p. 310, muon Decay.

[14] T. van Ritbergen and R. G. Stuart, On the precise determination of the fermi coupling constant from the muon lifetime, Nuclear Physics B **564**, 343–390 (2000).

[15] H. Fujii, K. Hara, K. Hayashi, H. Kakuno, H. Kodama, K. Nagamine, K. Sato, S.-H. Kim, A. Suzuki, T. Sumiyoshi, K. Takahashi, F. Takasaki, S. Tanaka, and S. Yamashita, Investigation of unit-1 nuclear reactor of the fukushima daiichi by cosmic muon radiography (2020), arXiv:2003.02057 [physics.ins-det].

[16] T. Ward, M. Barker, J. Breeden, K. Komisarcik, M. Pickar, D. Wark, and J. Wiggins, Laboratory study of the cosmic-ray muon lifetime, American Journal of Physics **53**, 542 (1985), https://pubs.aip.org/aapt/ajp/article-pdf/53/6/542/11848928/542_1_online.pdf.

[17] A. Owens and A. E. Macgregor, Simple technique for determining the mean lifetime of the cosmic ray meson, American Journal of Physics **46**, 859 (1978), https://pubs.aip.org/aapt/ajp/article-pdf/46/8/859/12028913/859_1_online.pdf.

[18] T. Coan, T. Liu, and J. Ye, A compact apparatus for muon lifetime measurement and time dilation demonstration in the undergraduate laboratory, American Journal of Physics **74**, 161 (2006), https://pubs.aip.org/aapt/ajp/article-pdf/74/2/161/16717708/161_1_online.pdf.

[19] B. Brau, C. May, R. Ormond, and J. Essick, Determining the muon mass in an instructional laboratory, American Journal of Physics **78**, 64–70 (2009).

[20] D. E. Groom and S. Klein, Passage of particles through matter, The European Physical Journal C-Particles and Fields **15**, 163 (2000).

[21] National Institute of Standards and Technology, CODATA Value: Muon Mass Energy Equivalent in MeV (2025), the NIST Reference on Constants, Units, and Uncertainty.